Dissipativity Analysis of the Base Isolated Benchmark Structure with MR Fluid Dampers

Baris Erkus[1] and Erik A. Johnson[2]

ABSTRACT

This paper investigates the dissipativity and performance characteristics of the semiactive control of the base isolated benchmark structure with MR fluid dampers. Previously, the authors introduced the concepts of dissipativity and dissipativity indices in semiactive control of structures with smart dampers and investigated dissipativity characteristics of simple structures with idealized dampers. To investigate the effects of dissipativity characteristics of semiactive controller on the overall performance of the base isolated benchmark building, a clipped optimal control strategy with a LQG controller and a 20 ton MR fluid damper model is used. A cumulative index is proposed to quantify the overall dissipativity of a control system with multiple control devices. Two control designs with different dissipativity and performance characteristics are considered as the primary controller in a clipped optimal control. Numerical simulations reveal that the dissipativity indices can be classified into two groups that exhibit two distinct patterns. It is shown that the dissipativity indices identify primary controllers that are more suitable for application with MR dampers and provide useful information in the semiactive design process that compliments other performance indices. Computational efficiency of the proposed dissipativity indices is verified by comparing computation times.

Keywords: dissipativity indices, smart dampers, benchmark problem, clipped optimal control

INTRODUCTION

In the last decade, semiactive control of civil structures with smart dampers for seismic protection received special attention in the structural control community (Housner *et al.*, 1997; Spencer and Sain, 1997; Symans and Constantinou, 1999; Soong and Spencer, 2002). It has been shown by various researchers that smart dampers have attractive performance, robustness and reliability properties that make them a sound alternative to active and passive control for seismic hazard mitigation (Dyke *et al.*, 1996; Taylor and Constantinou, 1996; Symans and Constantinou, 1998; Gavin, 2001; Erkus *et al.*, 2002; Johnson *et al.*, 2007; Ok *et al*., 2007; Rodriguez *et al*. 2010).

1. Engineer, Arup, Los Angeles, CA 90066; Baris.Erkus@arup.com. Previously graduate student at Univ. of Southern California.
2. Assoc. Prof., Dept. of Civil and Env. Engrg., Univ. of Southern California, Los Angeles, CA 90089-2531; JohnsonE@usc.edu

One popular approach for commanding a smart damper is clipped optimal control (Dyke *et al.,* 1998; Spencer *et al.*, 2000; Erkus *et al.,* 2002; Ramallo *et al.*, 2002; Johnson *et al.,* 2007). Clipped optimal control is a two-stage control approach, where an optimal linear quadratic control theory is used to design a primary controller, and a bang-bang type clipping algorithm commands the damper such that it mimics the primary controller force as close as possible. In general, the design of a clipped optimal controller involves two steps. In the first step, a primary controller is designed to achieve a predefined design goal assuming that structure is linear and the smart damper is an active device. In the second step, the complete semiactive system is simulated with the designed primary controller for several historical or predicted excitations. Several iterations performed to find the best primary controller that achieves the overall semiactive design goal.

The clipped optimal control strategy may have several challenges when applied to a real-life structural engineering problem, where it is quite common that the structure have a large complicated model with various irregularities. Further, the size of the structure requires utilization of many smart dampers that have sophisticated mathematical models. In these cases, primary controllers obtained in the first step of the clipped optimal control design may not achieve a satisfactory semiactive system. While this can be attributed to the complexity of the overall problem, the main assumption used in the first step of the semiactive design has also an important role on the efficiency of the primary controller within the semiactive system. Clearly, the primary controller can result both dissipative forces and forces that inject energy to the structure to achieve the design goals. On the other hand, a smart damper is a dissipative device, and it can not mimic the primary control forces if they are mostly nondissipative, which will result an inefficient semiactive system. Identification of the primary controllers that are well-suited for smart dampers only through numerical simulations without previously identifying the nondissipative controllers may be very time-inefficient due to the size of the structure and complicated models of the structure and dampers. Therefore, it is essential to understand the concept of dissipativity and its role within semiactive control of structures to design efficient semiactive controllers without conducting time-expensive simualtions.

Previously, several researchers investigated the dissipativity within the context of semiactive control of structures with smart dampers. Inaudi (2000), Aly and Christenson (2008) showed that certain primary controllers for a given design goal have higher probability of producing dissipative forces, and they are more effective in semiactive control of structures. Erkus *et al.* (2002) provided a numerical example where semiactive control is not effective for certain design objectives and observed that for these design goals primary controller have lower dissipativity levels. Some other studies investigated the capability of smart damping systems in achieving the performance of corresponding fully active systems (Ou and Li, 2010)

All these studies show that dissipativity measures are useful in understanding and predicting the performance of a semiactive system with smart dampers.

In a previous research, the authors introduced formal definition of dissipativity and several indices to quantify the dissipativity of a primary controller, and they employed these indices to modify the dissipativity nature of an optimal linear quadratic controller using linear matrix inequalities. (Johnson and Erkus, 2007). However, the structural systems used in this study were simple two-degree-of-freedom (2DOF) systems and an ideal damper (one that can exert the primary control forces exactly as long as it is dissipative). It is necessary that the efficiency of these indices in identifying the dissipative nature of a primary controller is investigated for realistic engineering structures using realistic damper models.

This paper investigates the dissipativity-performance relations in a realistic semiactive control problem with smart dampers to illustrate the usefulness of dissipativity indices in the design of the semiactive controller. For the purpose, the ASCE base-isolated benchmark building (Narasimhan *et al.*, 2006; Erkus and Johnson, 2006) is selected as a test-bed, and a mathematical model of a prototype 20 ton magnetorheological (MR) fluid damper (Yang *et al.*, 2002) is employed. The benchmark problem provides several performance indices for measuring the efficiency of the proposed controller. The overall building exhibits various practical challenges that are often encountered in practical structural engineering. Clipped optimal control is used as the primary controller, and the aforementioned semiactive control process is implemented to achieve two design goals, that are based on minimizing the base drifts and absolute floor accelerations. These design goals are frequently used in control of base-isolated building and, further, it is a common sense that these design goals will result primary controllers that exhibit high and low dissipativity characteristics. Therefore they are good candidates for the purpose of this study. As part of the first step of the semiactive design, two primary active controllers are obtained by considering fully active systems that achieves the two design goals. Then, the overall semiactive systems are simulated using the primary controllers obtained in the first step. The performance indices obtained in the first and second steps are presented. Finally, the dissipativity indices are obtained at the first and second steps of the design process for the two designs and their relations to performance indices are investigated. Various other advantages of the dissipativity indices, such as time efficiency, and capability of identifying dampers that operates more effectively, are identified.

BACKGROUND

In this section, a brief review of the previously defined dissipativity indices, base isolated benchmark structure and the optimal linear quadratic controller used as a primary controller are given. The reader is referred to the relevant literature for further details.

Dissipativity Indices

Let the primary control force in a clipped optimal control strategy be denoted u_a, and the corresponding velocity across the damper be v_d. For a given excitation, a deterministic dissipativity index can be defined as

$$D_{\%} = 1 - \frac{1}{T}\int_0^T H[u_a v_d]dt \tag{1}$$

where $H[\cdot]$ is the Heaviside unit step function, u_a is the primary control force, v_d is the damper velocity and $D_{\%}$ is the percentage of the dissipative primary control forces. Another deterministic dissipativity index, which is used in the benchmark problem (Narasimhan *et al.*, 2006), is

$$D_{\text{nedcf}} = \frac{E_{\text{dissipated}}}{E_{\text{input}}} \tag{2}$$

where $E_{\text{dissipated}}$ is the energy dissipated by the control force, E_{input} is the energy input to the system by the excitation, and D_{nedcf} is the normalized energy dissipated by the control force. For a linear system with stationary Gaussian responses, a stochastic dissipativity index can be defined as the probability that the control force is strictly dissipative (Inaudi, 2000)

$$D_p = P[u_a v_d < 0] = \frac{\operatorname{acos}(\rho_{u_a v_d})}{\pi} \tag{3}$$

where $\rho_{u_a v_d}$ is the correlation coefficient between the primary control force u_a and the damper velocity v_d. The authors have previously proposed the following two statistical indices (Johnson and Erkus, 2007):

$$D_e = E[u_a v_d] \qquad \text{and} \qquad D_{ne} = \frac{E[u_a v_d]}{\sqrt{E[u_a^2]}\sqrt{E[v_d^2]}} \tag{4}$$

where $E[\cdot]$ is the expected value, D_e is the mean energy flow rate and D_{ne} is the normalized mean energy flow rate. Note that D_{ne} is the correlation coefficient between u_a and v_d; *i.e.*, $D_{ne} = \rho_{u_a v_d}$.

The mathematical model of the benchmark structure is given by (Erkus and Johnson, 2006). The damper model used in this study is developed by Yang *et al.* (2002) for a 20 ton prototype MR fluid damper. A linear quadratic Gaussian similar to the controller defined by Erkus and Johnson (2006) is used as the primary controller. These model and controller equations are well-documented will not be repeated herein. The schematic representation of the resulting semiactive system is shown in Figure 1.

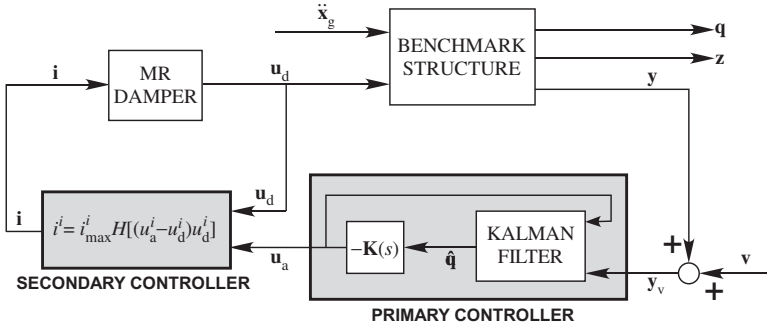

FIG. 1 Clipped optimal control of the benchmark structure.

SEMIACTIVE CONTROL OF THE BENCHMARK STRUCTURE

In this section, clipped optimal control is applied to the benchmark structure for commanding MR fluid dampers. Various aspects of the primary controller used in this study (Kalman estimator, measured quantities, Kanai-Tajimi filter and etc.) is similar to controller defined in the benchmark paper by Erkus and Johnson (2006), and will not be repeated here. Two control design goals are introduced based on the performance indices defined in the original benchmark study (Narasimhan *et al.*, 2006). A conventional approach is used to design the primary controller to satisfy the chosen design goals, and the semiactive system is simulated using the resulting clipped optimal controller. Performance indices are presented graphically and tabularly for both active and semiactive structures.

To facilitate the investigation of the dissipativity indices for controllers with high and low dissipativity characteristics, the outputs to be minimized are selected as $\mathbf{z} = [(\mathbf{x}^{coriso})^T \ (\ddot{\mathbf{x}}^{abs})^T]^T$ where $\mathbf{x}^{coriso} = [d\mathbf{X}_b]$ are the corner isolator drifts and $\ddot{\mathbf{x}}^{abs}$ are the absolute accelerations of the floor center-of-masses. The control design parameters $\mathbf{Q}$, $\mathbf{R}$ and $\mathbf{N}$ are selected as explained in the benchmark paper as follows (Erkus and Johnson, 2006):

$$\mathbf{Q} = b\begin{bmatrix} a\alpha & \\ & \beta \end{bmatrix}, \qquad \mathbf{R} = r\mathbf{I}, \qquad \mathbf{N} = \mathbf{0} \tag{5}$$

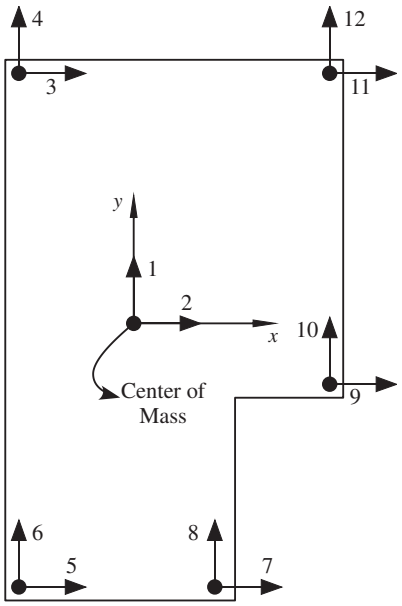

FIG. 2 Locations of the controllers.

This set of parameters reduces the control design problem to a choice of the parameters a and b, which determine the relative importance of the corner drifts and absolute floor accelerations. Twelve control devices are used and located as shown in Figure 2.

There are various performance indices defined in the original benchmark problem definition paper (Narasimhan *et al.*, 2006), and two new indices introduced in the bilinear phase (Erkus and Johnson, 2006). These performances indices are summarized in Table 1; note that the index J_9 is same as the dissipativity index D_{nedcf}.

Seven earthquake ground motion data with two components — fault-normal and fault-parallel — are used in the numerical simulations. These are summarized in Table 2. Details of these data can be found in the benchmark definition paper (Narasimhan *et al.*, 2006).

Two design goals are considered for the semiactive clipped optimal control. The first design aims to reduce peak base drift J_3; the resulting design is denoted DESDRIFT. The second design aims to reduce peak absolute floor accelerations J_5; the design is denoted DESACCEL. To reach these goals, a conventional clipped optimal control design approach is followed: a fully active system is designed to achieve the corresponding design goal and this active controller is used as the primary controller in the clipped optimal control. The active controller parameters a and b can be designed in many ways. In this study, active control designs that satisfy a set of predefined conditions on performance indices, which are shown in Table 3, for each of the seven earthquake data are found with a numerical study. These predefined conditions are: to

minimize either J_3 or J_5 while keeping the other as good or better than with the nominal (passive) isolation system, as well as keeping the peak superstructure interstory drift as good or better than with the nominal isolation and insuring that the peak combined force of all devices at base center is no more than 15% of the weight of the building (a typical value for isolation designs for strong earthquakes; Ramallo *et al.*, 2002).

The parameters a and b that corresponds to these seven active designs are called *best designs.* The logarithms (base 10) of each of the seven best design parameters are then averaged to obtain a final a and

TABLE 1: Definitions of the performance indices

J	Definition
J_1	Peak Base Shear
J_2	Peak First Floor Shear
J_3	Peak Base Drift
J_4	Peak Interstory Drift
J_5	Peak Absolute Floor Acceleration
J_6	Peak Control Device Force
J_7	RMS Base Drift
J_8	RMS Absolute Floor Acceleration
J_9	Energy Absorbed by the Control Devices
J_{10}	Normalized Peak Control Device Force[a]
J_{11}	RMS Floor Drifts

a. This index is different than J_6; see Narasimhan *et al.* (2006) and Erkus and Johnson (2006) for definitions.

TABLE 2: Earthquake ground motion data used in the numerical simulations

Earthquake	Location
Northridge, California (1994)	Newhall
	Sylmar
	Rinaldi
Imperial Valley, California (1940)	El Centro
Kobe, Japan (1995)	Kobe
Jiji, Taiwan (1999)	Jiji
Erzincan, Turkey (1992)	Erzincan

b pair for each design goal; the corresponding design is called the *final design*. The results of this parametric study is shown in Table 4.

The control design for the benchmark building is a very complex trade-off problem, and various design approaches may yield different designs. To illustrate this challenge and to observe the general trends of the performance indices, the best and the final control designs for DESDRIFT are graphed along with some of the performance indices for the Newhall earthquake data in Figure 3. It is easy to observe that peak shear indices J_1 and J_2 show trends similar to peak acceleration J_5. Likewise, peak base and interstory drifts indices J_3 and J_4 have similar behavior, and are both a trade-off relative to the shear and acceleration indices. Thus, any design that favors one group of indices compromises the other group. Moreover, they will show different behaviors for different earthquakes.

To further explain the trade-off between DESDRIFT and DESACCEL, base drift index J_3 and superstructural acceleration index J_5 are graphed in separate figures for several other earthquakes in Figure 4. The contour graphs prove the challenge associated with the trade-off problem discussed previously. For example, if a design is selected for DESDRIFT based on a single earthquake, the design will likely not be

TABLE 3: Conditions on the performance indices for control designs

J	DESDRIFT	DESACCEL
J_3	min (J_3)	$J_3 < 1.0$
J_4	$J_4 < 1.0$	
J_5	$J_5 < 1.0$	min (J_5)
J_{10}	$J_{10} < 0.15$	

TABLE 4: Best and final controller design parameters

Earthquake	DESDRIFT		DESACCEL	
	$\log_{10}(a)$	$\log_{10}(b)$	$\log_{10}(a)$	$\log_{10}(b)$
Newhall	–2.1429	–0.9184	–3.9796	–0.7143
Sylmar	–2.7551	–0.7143	–3.3673	–0.1020
El Centro	–1.7347	–0.5102	–3.1633	–1.1224
Rinaldi	–2.5510	–0.9184	–2.7551	–0.7143
Kobe	–2.1429	–1.3265	–3.3673	–0.3061
Jiji	–1.3265	–1.7347	–2.9592	–1.3265
Erzincan	–1.9388	–1.1224	–2.9592	–0.1020
Final	–1.9096	–1.0933	–3.2216	–0.3061

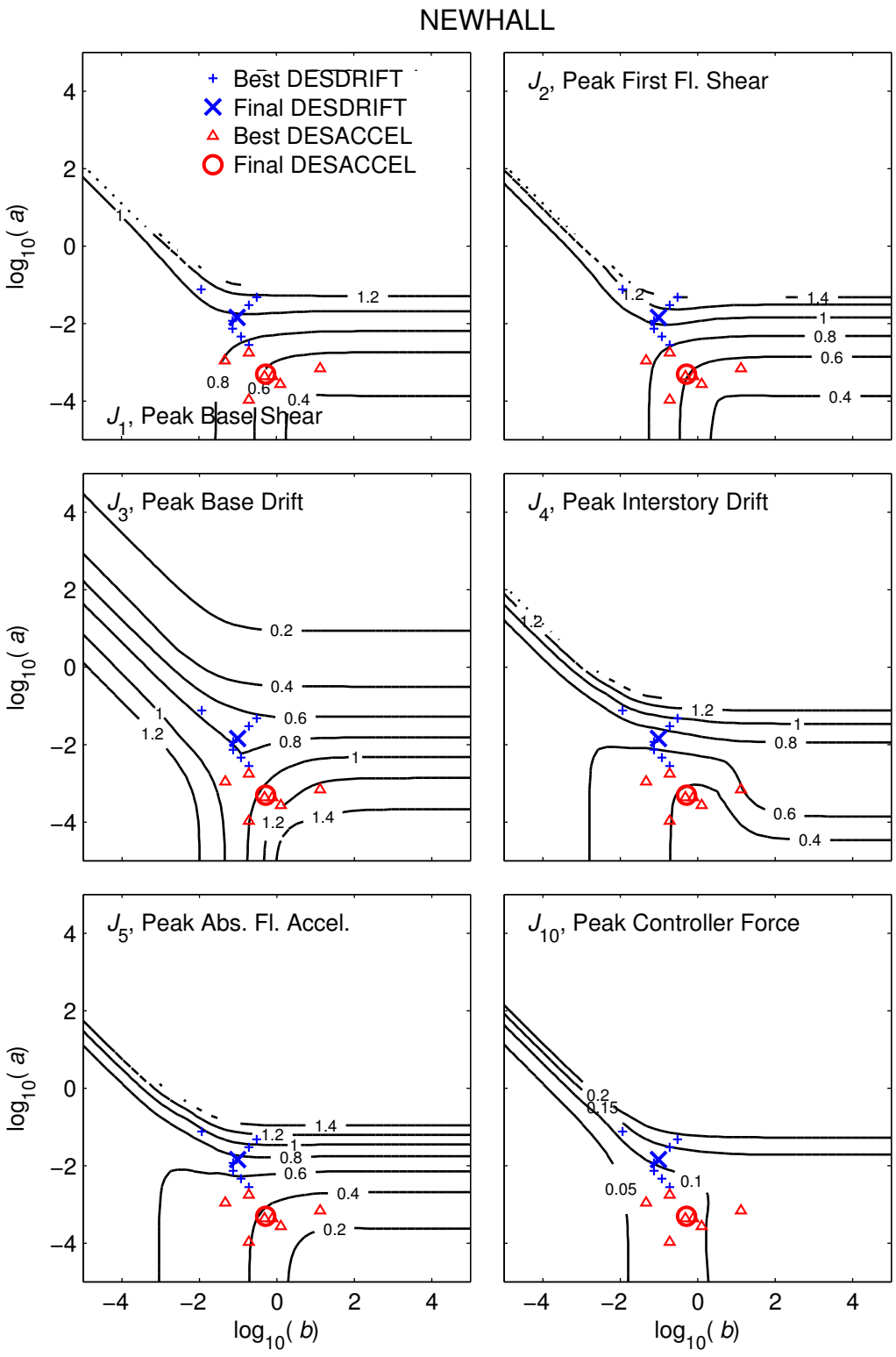

FIG. 3 Best and final designs and various performance indices for Newhall earthquake

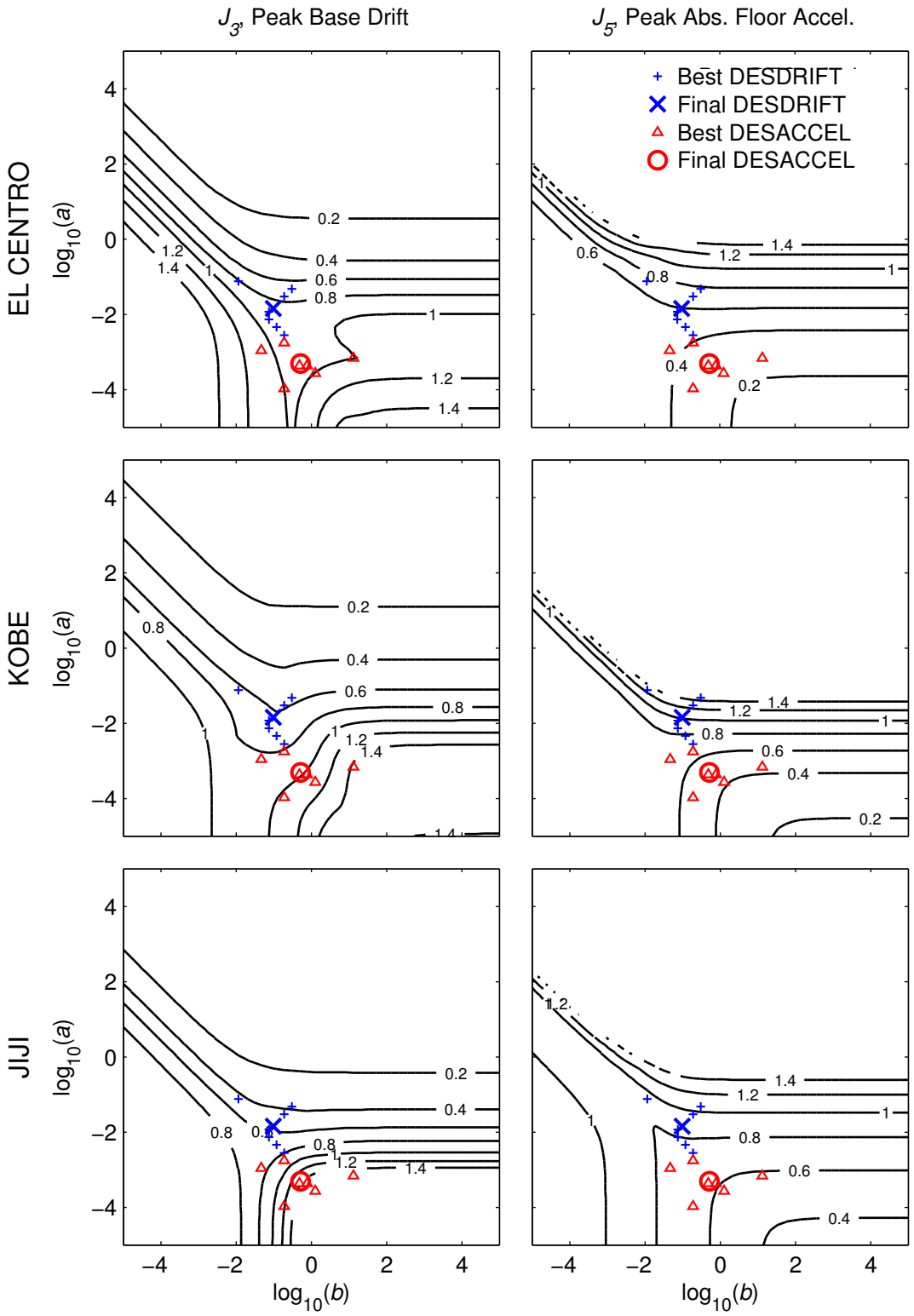

FIG. 4 Best and final designs and performance indices J_3 (base drift) and J_5 (floor accelerations) for El Centro, Kobe and Jiji earthquakes

TABLE 5: Performance indices, active and semiactive, with the DESDRIFT primary controller.

J		Newhall		Sylmar		El Centro		Rinaldi		Kobe		Jiji		Erzincan	
(Normalized with appropriate quantities)		ACT	SAct	ACT	SAct	ACT	SAct	ACT	SAct	ACT	SAct	ACT	SAct	ACT	SAct
J_1	Peak Base Shear	0.969	0.979	0.929	1.019	0.856	0.943	1.203	1.295	1.133	1.150	0.742	0.806	1.024	0.983
J_2	Peak 1st Floor Shear	1.071	1.188	1.005	1.087	0.914	0.965	1.210	1.302	1.183	1.160	0.766	0.802	1.028	0.994
J_3	Peak Base Drift	0.764	0.854	0.656	0.795	0.862	0.852	0.809	0.834	0.620	0.645	0.549	0.531	0.552	0.618
J_4	Peak Interstory Drift	0.689	1.103	1.169	1.338	0.725	0.930	1.204	1.284	1.139	1.568	0.821	0.876	1.006	1.032
J_5	Peak Absolute Floor Acceleration	0.750	1.087	1.309	1.580	0.594	1.122	1.226	1.507	1.012	1.559	0.861	0.965	0.984	1.021
J_6	Peak Controller Force	0.624	0.552	0.634	0.599	0.527	0.587	0.805	0.740	0.732	0.769	0.408	0.328	0.525	0.546
J_7	RMS Base Drift	0.774	0.848	0.606	0.747	0.904	0.854	0.692	0.777	0.748	0.709	0.617	0.563	0.519	0.606
J_8	RMS Absolute Floor Acceleration	0.804	1.110	0.799	0.996	0.564	0.929	1.069	1.240	0.830	1.232	0.743	0.820	0.768	0.840
J_9	Energy Absorbed by the Control Devices	0.701	0.718	0.740	0.737	0.713	0.750	0.735	0.732	0.675	0.723	0.740	0.720	0.758	0.747
J_{10}	Normalized Peak Controller Force	0.111	0.099	0.150	0.142	0.044	0.049	0.194	0.178	0.099	0.104	0.155	0.124	0.115	0.120
J_{11}	RMS Floor Drifts	0.876	1.026	0.813	0.869	0.583	0.790	1.078	1.128	0.909	1.155	0.733	0.786	0.771	0.817

optimal for other earthquakes. Moreover, it is very likely that a good DESDRIFT will have a poor, in some cases unacceptable, peak acceleration J_5.

Next, in the semiactive design, the final active controllers are used as primary controllers in the clipped optimal control. Since the capacity of a single 20 ton MR fluid damper provides insufficient force levels for this structure, the MR fluid damper model force is magnified by a factor in the semiactive simulations to simulate the use of a larger MR fluid damper (or several 20 ton dampers working together). After some test simulations, it is found that a factor of 8 is appropriate for the DESDRIFT primary controller and a factor of 5 for DESACCEL. The benchmark structure with smart dampers is simulated for each of seven different earthquake ground motion time histories; the performance indices with the DESDRIFT active and clipped optimal control strategies are shown in Table 5, and those with the DESACCEL strategy are in Table 6.

Table 5 shows that clipped optimal control is very effective in mimicking the primary control force for DESDRIFT, resulting in performance indices (particularly the base drift index J_3) comparable to the corresponding fully active system. As DESDRIFT attempts to reduce the base drift J_3, with no regard for the peak accelerations J_5, it is of little surprise that the semiactive DESDRIFT strategy has large accelerations J_5 for some earthquakes. Also, Figure 4 shows that the performance index trade-offs are sensitive in that a

TABLE 6: Performance indices, active and semiactive, with the DESACCEL primary controller.

J		Newhall		Sylmar		El Centro		Rinaldi		Kobe		Jiji		Erzincan	
(Normalized with appropriate quantities)		ACT	SAct	ACT	SAct	ACT	SAct	ACT	SAct	ACT	SAct	ACT	SAct	ACT	SAct
J_1	Peak Base Shear	0.581	1.058	0.543	1.046	0.515	1.066	0.715	1.317	0.636	1.166	0.597	0.945	0.557	1.132
J_2	Peak 1st Floor Shear	0.611	1.240	0.583	1.183	0.514	1.039	0.710	1.442	0.644	1.149	0.607	0.917	0.558	0.998
J_3	Peak Base Drift	1.047	0.972	0.930	0.917	0.889	1.057	1.169	0.951	0.979	0.789	1.364	0.615	0.833	0.730
J_4	Peak Interstory Drift	0.379	1.123	0.695	1.297	0.375	0.962	0.693	1.277	0.597	1.461	0.640	0.911	0.612	0.916
J_5	Peak Absolute Floor Acceleration	0.372	1.157	0.699	1.545	0.292	1.120	0.653	1.625	0.504	1.438	0.636	1.102	0.527	1.071
J_6	Peak Controller Force	0.488	0.473	0.531	0.504	0.426	0.423	0.535	0.624	0.417	0.677	1.024	0.328	0.427	0.379
J_7	RMS Base Drift	1.034	1.025	0.755	0.925	1.444	1.068	0.969	0.977	1.060	0.885	1.674	0.639	0.704	0.767
J_8	RMS Absolute Floor Acceleration	0.423	1.066	0.421	0.999	0.322	0.911	0.553	1.165	0.411	1.157	0.636	0.877	0.416	0.877
J_9	Energy Absorbed by the Control Devices	0.477	0.651	0.504	0.649	0.521	0.678	0.548	0.650	0.416	0.656	0.605	0.649	0.541	0.655
J_{10}	Normalized Peak Controller Force	0.087	0.084	0.126	0.120	0.035	0.035	0.129	0.150	0.056	0.091	0.389	0.125	0.094	0.083
J_{11}	RMS Floor Drifts	0.502	1.003	0.514	0.882	0.327	0.769	0.594	1.060	0.502	1.092	0.580	0.837	0.503	0.860

small change in one index may result in a large increase or decrease of the other index. Overall, the semiactive system performance can be considered efficient in achieving the DESDRIFT design goals.

On the other hand, Table 6 shows that the semiactive system is not successful compared to the active system for DESACCEL. The DESACCEL design objective to reduce peak acceleration J_5 is achieved for the active system, but this performance is not reflected in the semiactive system. The energy absorbed J_9 with the DESACCEL design is clearly smaller than that with the DESDRIFT design; in other words, the DESDRIFT design commands forces more dissipative than DESACCEL, resulting in the DESDRIFT controller being more suitable for MR fluid dampers than DESACCEL. DESACCEL does not have the necessary characteristics to make it suitable for the damper by nature and should not be considered for semiactive design. Thus, the energy absorbed index J_9 provides information that can be very useful in the design process.

However, while energy absorbed J_9 is a useful indicator of how efficient an active control design can be implemented with a semiactive damper, it is not an indicator easy to use. It is a deterministic value based on the response to a specific excitation time history. Thus, it is earthquake dependent and results may vary from one earthquake to another. Further, it requires simulating the active system, which may be time–consuming for complex structural systems. In the following section, other dissipativity indices that does

not require extensive numerical simulations and that may provide information similar to energy absorbed index J_9 are investigated.

DISSIPATIVITY ANALYSIS OF THE BENCHMARK STRUCTURE

In this section, a detailed dissipativity analysis of the benchmark structure is provided. First, characteristics of the selected control strategies, DESDRIFT and DESACCEL, are investigated using the proposed dissipativity indices. Since the dissipativity indices previously discussed in the Background section are for single control devices, a cumulative index is proposed to compute a dissipativity index for a system with multiple control devices. Then, to further exploit the dissipativity-performance relations, the two sets of control designs with various characteristics are investigated in detail.

Cumulative Dissipative Indices

The dissipativity indices, except D_{nedcf}, are for systems with a single controller and cannot be directly used for the control strategies previously discussed for the benchmark problem since they have multiple control devices. A cumulative index is defined here to represent the dissipativity characteristics of the control designs as follows:

$$D^{\text{c}} = \sum_{i=1}^{N} w_i D_i \tag{6}$$

where D^{c} is a cumulative dissipativity index that is a weighted average of individual dissipativity indices D_i of the N control devices, weighted by the relative RMS force of the i^{th} device:

$$w_i = \frac{\text{RMS}[u_i]}{\sum_{j=1}^{N} \text{RMS}[u_j]} \tag{7}$$

To understand the general dissipative characteristics of the active control designs DESDRIFT and DESACCEL, the dissipativity indices of the individual controllers and the cumulative dissipative indices are computed and shown in Tables 7 and 8. The first observation regarding these results is that the proposed cumulative indices are good indicators of the overall dissipativity characteristics of the control designs, and they can be used in place of the individual controller dissipativity indices. It is also observed that some of the controllers of the active system have lower dissipativity indices compared to the others (*e.g.*, devices 5, 7, 10 and 12). Considering the locations of these dampers (Figure 2) and the irregular

shape of the structure, one can judge that some of the smart dampers may not be as efficient as others because of the torsional irregularity of the benchmark structure. This information is very useful in the sense that the designer may now choose to remove or relocate these dampers to obtain better dissipativity characteristics; alternately, active or passive devices may be used instead of the smart dampers.

It is also observed from Tables 7 and 8 that DESDRIFT has a more dissipative nature than DESACCEL. This is true for both active and semiactive systems. One important difference between these two designs is that the dissipativity indices of the active system give a reasonably good sense of what the semiactive dissipativity indices will be for the DESDRIFT control design. On the other hand, this is not true for the DESACCEL case. As discussed previously, the reason for this is that semiactive system with DESACCEL controller is not successful in realizing the active system due to the poor dissipative nature of the controller; therefore, performance and dissipativity indices of the semiactive system become different than the active system for the DESACCEL case compared to DESDRIFT. Considering these results and the performance indices reported in Tables 5 and 6, one can conclude that both individual and cumulative dissipativity indices are successful in predicting the dissipative nature of the primary controller and provide useful information about performance of the semiactive system without extensive numerical simulations. Therefore, dissipativity indices can be used to select primary controllers those are more suitable for the clipped optimal control of a structure.

TABLE 7: DESDRIFT dissipativity indices.

i	$D_{\%}$[a]		D_e	D_{ne}
	Act	SAct	Act	Act
1	0.900	0.878	–1348	–0.865
2	0.873	0.838	–1349	–0.853
3	0.900	0.880	–1665	–0.883
4	0.873	0.828	–1504	–0.860
5	0.782	0.800	–934	–0.707
6	0.873	0.828	–1504	–0.860
7	0.782	0.800	–934	–0.707
8	0.862	0.837	–1245	–0.837
9	0.875	0.870	–1242	–0.845
10	0.813	0.798	–1090	–0.788
11	0.900	0.880	–1665	–0.883
12	0.813	0.798	–1090	–0.788
D^c	0.859	0.844	–1324	–0.828

a.Computed for the Newhall data

TABLE 8: DESACCEL dissipativity indices.

i	$D_{\%}$[a]		D_e	D_{ne}
	Act	SAct	Act	Act
1	0.633	0.693	–1101	–0.247
2	0.640	0.723	–1046	–0.244
3	0.550	0.692	–1216	–0.237
4	0.617	0.690	–1139	–0.238
5	0.602	0.645	–751	–0.173
6	0.617	0.690	–1139	–0.238
7	0.602	0.645	–751	–0.173
8	0.565	0.717	–962	–0.238
9	0.648	0.700	–1038	–0.240
10	0.545	0.702	–794	–0.205
11	0.550	0.692	–1216	–0.237
12	0.545	0.702	–794	–0.205
D^c	0.588	0.688	–1012	–0.225

a.Computed for the Newhall data

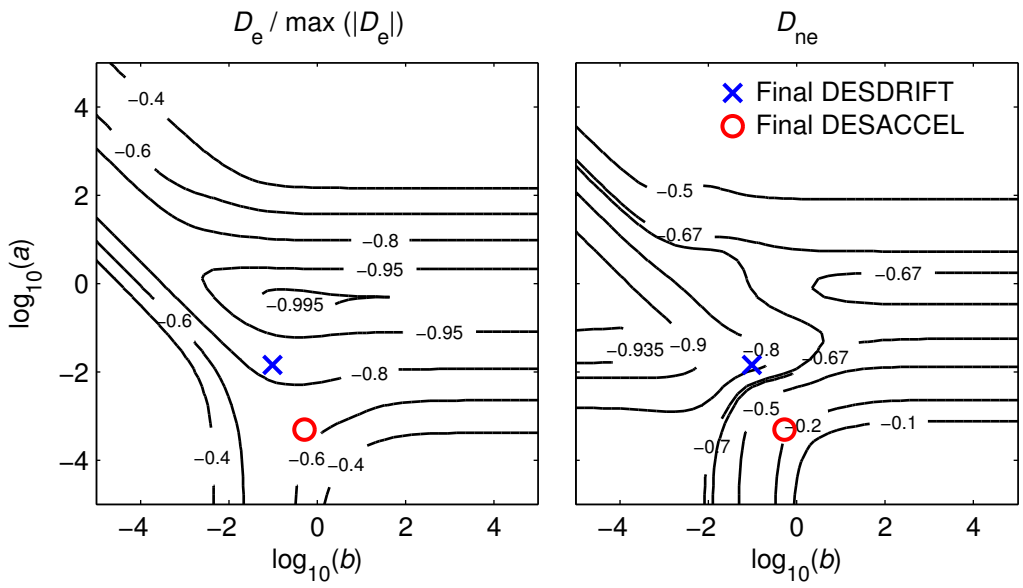

FIG. 5 D_e and D_{ne} plots for the active structure.

Classification of Dissipativity Indices

The results and observations given above suggest that the dissipativity of the controllers is useful in understanding the performance indices given in Figure 3. In this respect, the cumulative dissipativity indices are graphed in Figures 5 and 6 in a manner similar to Figure 3.

An important observation of the dissipativity indices is the similarities between the patterns of D_{ne} and $D_{\%}$, and between D_e and J_9. To understand these similarities, consider the definitions of the dissipativity indices. In the first similarity, D_{ne} is the correlation coefficient between the control force and the velocity; therefore, D_p is the cosine of D_{ne}. Since D_p is the probability of the control force being dissipative, and since $D_{\%}$ is the same probability obtained approximately through numerical experiments, one can justify the similarity between $D_{\%}$ and D_{ne}. The similarity between D_e and J_9 can also be explained in a similar manner: since J_9 is a normalized time integral of energy flow rate, D_e is proportional to the mean of J_9 for a white-noise excitation. It should, however, be noted that these similarities are observed in the patterns of the contour plots of the indices but not directly with their values. Based on these relations, a classification of the indices is provided in Table 9, with which one can determine the general trends of all of the dissipativity indices by computing two of them, one from each group.

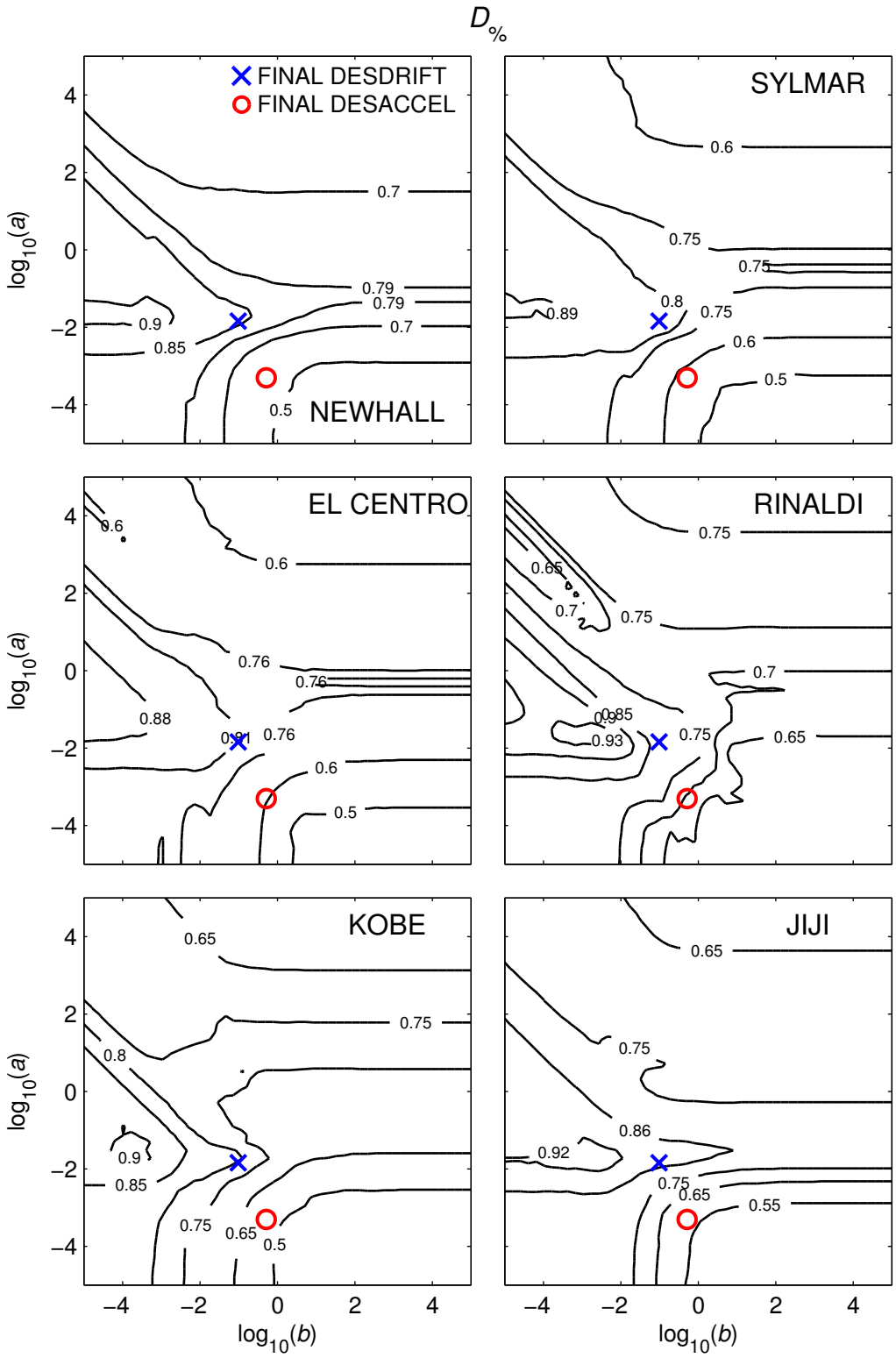

FIG. 6 $D_{\%}$ plots for the active structure

Dissipativity-Performance Relations

In this section, a discussion of the relations between dissipativity and performance of the benchmark structure is provided, first considering the performance and dissipativity tables and plots provided in the previous section, then conducting a more detailed numerical study.

It is observed from Figures 3, 4, 5 and 6 that the active control designs with the highest dissipativity indices have either very large active base drift J_3 or very large active absolute floor acceleration J_5. Therefore, although the primary controllers that use these active designs may be suitable for MR fluid dampers to successfully mimic the primary control force, they would most probably result in unacceptable overall semiactive performance. This shows that high dissipativity values do not necessarily imply better overall semiactive performance since, generally, semiactive clipped system performance is always bounded by the corresponding active system performance. These simulations, therefore, suggest that an active primary controller for a semiactive system should be designed both considering the active performance and the dissipativity of the controller.

To further elaborate on the relations between dissipativity and performance indices, the performance and dissipativity characteristics of the control designs that fall between the final DESDRIFT and DESACCEL designs in the (a, b) parameter space, and control designs located away from the final DESDRIFT and DESACCEL designs, are investigated. For this purpose, two families of active control designs, defined by 'Line A' and 'Line B', are considered as shown on the contour plot of active base drift J_3 in Figure 7. Active control designs on Line A represent the transition between final DESDRIFT and DESACCEL designs, whereas Line B represents active controllers with uniformly varying base drift J_3 and superstructure absolute acceleration J_5 indices. Since, as explained previously, DESDRIFT uses an MR fluid damper magnification factor of 8 and DESACCEL uses 5, the magnification factor along Line A is taken to lin-

TABLE 9: A Classification of dissipativity indices

	Definition of the Dissipativity Index	**Dissipativity Index**
GROUP 1	Normalized mean energy dissipation rate	D_{ne}
	Percentage of dissipative forces	$D_{\%}$
	Probability of dissipative forces	D_{p}
GROUP 2	Energy dissipation rate	D_{e}
	Normalized energy dissipated by the device	$D_{\mathrm{nedcf}}\,(J_9)$

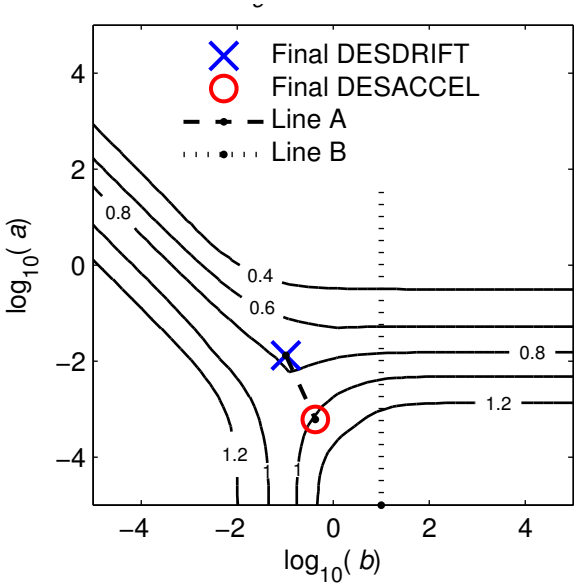

FIG. 7 Locations of Lines A and B on the active base drift J_3 contour plot.

early vary with distance in the log-log (a, b) space. For line B, the magnification factor is 5 for all of the controllers. The dissipativity and performance characteristics of the controllers on Lines A and B are shown in Figure 8 for the Newhall earthquake excitation. Note that, to facilitate visualization of all dissipativity indices on the same graphs, dissipativity index D_{e} is normalized by its maximum absolute value and $D_{\%}$ is negated.

It is immediately observed from Figure 8 that dissipativity indices of both semiactive and active systems along Line A show similar behavior: high dissipativity for DESDRIFT and lower dissipativity for DESACCEL. The transitions of active base drift J_3 and acceleration J_5 from DESDRIFT to DESACCEL are easily observed: better active acceleration J_5 is achieved by controllers with low dissipativity values. The semiactive system has a good base drift $(J_3)^{\mathrm{SAct}}$ for DESDRIFT, yet $(J_3)^{\mathrm{SAct}}$ increases with the decreasing dissipativities. It is also observed that semiactive absolute floor acceleration $(J_5)^{\mathrm{SAct}}$ is always larger than 1 and does not show a particular trend. The normalized peak control forces, measured by index J_{10}, also show similar trends. Therefore, the effect of the control force magnitudes when comparing active and semiactive characteristics is minimal.

The dissipativity and performance plots for Line B are more complicated, due primarily to the rapidly changing performance and control force magnitude indices. Along Line B, active $D_{\%}$ and D_{ne} indices are quite similar to each other. The semiactive dissipativity index $(D^{\mathrm{c}}_{\%})^{\mathrm{SAct}}$ shows a similar trend to $D_{\%}$ and D_{ne} for a range of control parameters. It is observed that primary control designs that are more suitable for

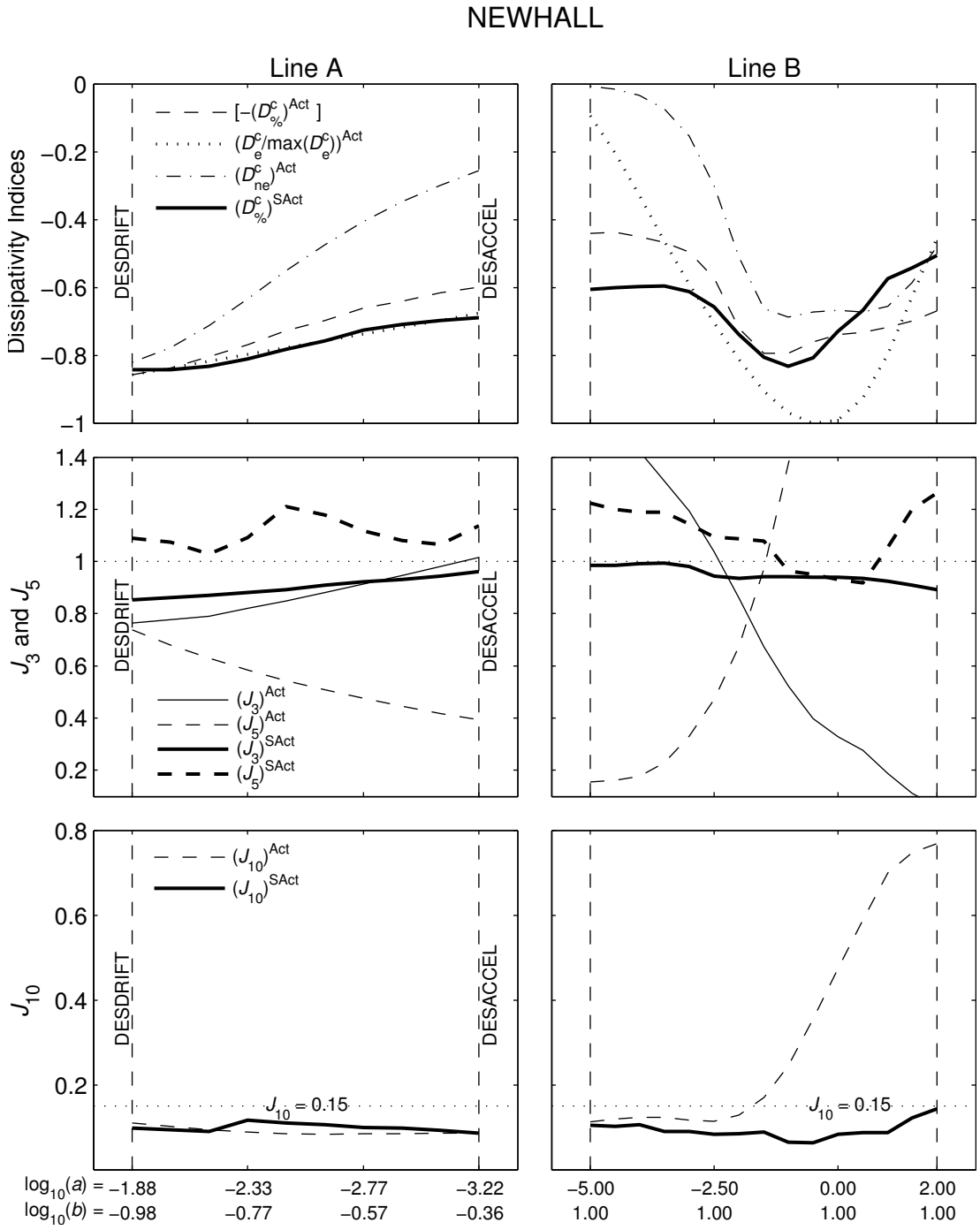

FIG. 8 Dissipativity and performance characteristics of the control designs along Lines A and B.

TABLE 10: Summary of the computational costs of dissipativity indices.

Dissipativity Indices	Computation Time [s]
Active Deterministic Indices, $(D_{\%})^{\mathrm{Act}}$, $(J_9)^{\mathrm{Act}}$	~ 600
Semiactive Deterministic Indices, $(D_{\%})^{\mathrm{SAct}}$, $(J_9)^{\mathrm{SAct}}$	~ 14400
Active Stochastic Indices, $(D_{\mathrm{p}})^{\mathrm{Act}}$, $(D_{\mathrm{e}})^{\mathrm{Act}}$, $(D_{\mathrm{ne}})^{\mathrm{Act}}$	< 1

the semiactive control has $(J_{10})^{\mathrm{Act}}$ indices around 0.5, which is a large value and would normally be not accepted as a practical control design. On the other hand, these designs have higher dissipativity indices (see D_{e} index) and damper force levels that are practically acceptable. These results are compatible with the results reported by Johnson and Erkus (2007), where it is stated that D_{e} index is more successful than D_{ne} and $D_{\%}$ indices in identifying control designs that are more suitable for the semiactive damper. In overall, these plots show that the performance of the semiactive design is a function of both the performance of the primary controller and the dampers ability to mimic the primary controller. The performance of the primary controller can be measured efficiently with stochastic indices and the dissipativity indices, can be used to measure the ability of the dampers to realize the primary control force.

Computational Considerations in the Design Process

A very important benefit of the proposed dissipativity indices is the time-efficiency of their computation. To compute the time-history dependent energy absorbed J_9 and the fraction of time dissipative $D_{\%}$, the active system (linear or nonlinear) must be simulated for an excitation, which may take around 10 minutes on a moderate Pentium (*e.g.*, Pentium 4, 2.4 GHz processor) computer. For the semiactively controlled structure with twelve MR fluid dampers, simulating 30 seconds of response may take about 4 hours of computer time (with an acceptable trade-off between time step and integration accuracy). On the other hand, computation of dissipativity indices D_{e} and D_{ne} takes less than a second since they only require the solution of a Lyapunov equation. These results are summarized in Table 10. From this perspective, a dissipativity analysis with the proposed indices provides a tool to investigate control designs that are more suitable for semiactive control problems with smart dampers in a much more computationally efficient manner.

CONCLUSIONS

In this paper, dissipativity and performance relations are investigated, utilizing dissipativity indices, in clipped optimal control of the base isolated benchmark building with MR fluid dampers. Both the structure

and the dampers have realistic mathematical models and possess many real-life design challenges. A cumulative dissipativity index is introduced to capture the dissipativity of a control system with multiple controllers. It is shown numerically that the dissipativity indices can be classified into two groups: the first is normalized energy dissipated D_{ne}, probability of being dissipative D_{p} and percent time dissipative $D_{\%}$; the second group includes energy dissipated D_{e} and energy dissipated by the controller normalized by input energy D_{nedcf} . Two control designs are considered, one emphasizing base drift (DESDRIFT) the other absolute floor accelerations (DESACCEL). DESDRIFT has higher dissipativity indices than DESACCEL. The primary controller with higher dissipativity values is more suitable for application with MR fluid dampers, and the dampers can realize DESDRIFT more efficiently than DESACCEL. Therefore, it is concluded that semiactive control of this base isolated structure with smart dampers is more successful in reducing base drift than reducing absolute floor accelerations. Finally, it is shown that the statistical dissipativity indices proposed by the authors can be effectively used without conducting time-expensive numerical simulations and are, therefore, essential tools in the design of semiactive clipped-optimal structural control systems.

ACKNOWLEDMENTS

The authors gratefully acknowledge the support of this research by the National Science Foundation under CAREER grant CMS 00-94030, and by the U.S. Department of Transportation through grant 03-17 from the National Center for Metropolitan Transportation Research (METRANS).

REFERENCES

Aly, A. M., and Christenson, R.E. (2008) “On the Evaluation of the Efficacy of a Smart Damper: A New Equivalent Energy-Based Probabilistic Approach”, *Smart Materials and Structures*, **17**(4), 11 pp.

Dyke, S. J., Spencer, B. F., Jr., Sain, M. K., and Carlson J. D. (1996). “Modeling and Control of Magnetorheological Dampers for Seismic Response Reduction.” *Smart Materials and Structures*, **5**(5), 565–575.

Dyke, S. J., Spencer, B. F., Jr., Sain, M. K., and Carlson J. D. (1998). “An Experimental Study of MR Dampers for Seismic Protection.” *Smart Materials and Structures*, **7**(5), 693–703.

Erkus, B., Abé, M., and Fujino, Y. (2002). “Investigation of Semi-Active Control for Seismic Protection of Elevated Highway Bridges.” *Engineering Structures*, **24**(3), 281–293.

Erkus, B., and Johnson, E. A. (2006). "Smart Base Isolated Benchmark Building Part III: A Sample Controller for Bilinear Isolation," *Journal of Structural Control and Health Monitoring*, **13**(2–3), 605–625.

Gavin, H. P. (2001). "Control of Seismically Excited Vibration using Electrorheological Materials and Lyapunov Methods." IEEE Transactions on Control Systems Technology, **9**(1), 27–36.

Housner, G. W., Bergman, L. A., Caughey, T. K., Chassiakos, A. G., Claus, R. O., Masri, S. F., Skelton, R. E., Soong, T. T., Spencer, B. F., Jr., and Yao, T. P. (1997). "Structural Control: Past, Present, and Future." *Journal of Engineering Mechanics*, ASCE, **123**(9), 897–971.

Inaudi, J. A. (2000). "Performance of Variable-Damping Systems: Theoretical Analysis and Simulation." *Proceedings of 3rd International Workshop on Structural Control*, Paris, France, 301–316.

Johnson, E. A., Baker, G. A., Spencer, B. F., Jr., and Fujino, Y. (2007). "Semiactive Damping of Stay Cables." *Journal of Engineering Mechanics*, ASCE, **133**(1), 1–11.

Johnson, E. A., and Erkus B. (2007) "Dissipativity and Performance Analysis of Smart Dampers via LMI Synthesis." *Journal of Structural Control and Health Monitoring*, **14**(3), 471-496.

Narasimhan, S., Nagarajaiah S., Gavin, H. P., and Johnson, E. A. (2006). "Smart Base Isolated Building Part I: Problem definition," *Journal of Structural Control and Health Monitoring*, **13**(2–3), 573–588.

Ok, S.-Y., Kim, D.-S., Park, K.-S., and Koh, H.-M. (2006) "Semi-active Fuzzy Control of Cable-stayed Bridges using Magneto-rheological Dampers." *Engineering Structures*, **29**(5), 776-788.

Ou, J., and Li, H. (2010) "Analysis of Capability for Semi-active or Passive Damping Systems to Achieve the Performance of Active Control Systems." *Journal of Structural Control and Health Monitoring*, **17**(7) 778-794.

Ramallo, J. C., Johnson, E. A., and Spencer, B. F., Jr. (2002). "'Smart' Base Isolation Systems." *Journal of Engineering Mechanics*, ASCE, **128**(10), 1088–1099.

Rodríguez, A., Pozo, F., Bahar, A., Acho, L., Vidal, Y., and J. Rodellar. (2010) "Force-derivative Feedback Semi-active Control of Base-isolated Buildings using Large-scale MR Fluid Dampers.", *Structural Control and Health Monitoring*, DOI: 10.1002/stc.430.

Soong, T. T., and Spencer, B. F., Jr. (2002). "Supplemental Energy Dissipation: State-of-the-art and State-of-the-practice." *Engineering Structures*, **24**(3), 243–259.

Spencer, B. F., Jr., and Sain, M. K. (1997). "Controlling Buildings: A New Frontier in Feedback." *IEEE Control Systems Magazine*, **17(**6), 19–35.

Spencer, B. F., Jr., Johnson, E. A., and Ramallo, J. C. (2000). "'Smart' Isolation for Seismic Control." *JSME International Journal*, Series C, **43**(3), 704–711.

Symans, M. D., and Constantinou, M. C. (1999). "Semi-Active Control Systems for Seismic Protection of Structures: A state-of-the-art review." *Engineering Structures*, **21**(6), 469–487.

Taylor, D. P., and Constantinou, M. (1996). "Fluid Dampers for Applications of Seismic Energy Dissipation and Seismic Isolation." Technical Report, Taylor Devices, Inc., North Tonawanda, New York.

Yang, G., Spencer, B. F., Jr., Carlson, J. D., and Sain, M. K. (2002). "Large-Scale MR Fluid Dampers: Modeling and Dynamic Performance Considerations." *Engineering Structures*, **24**(3), 309–323.